Bonding structure of carbon nitride films by infrared ellipsometry

A. Laskarakis, S. Logothetidis, and M. Gioti
Department of Physics, Aristotle University of Thessaloniki, GR-54006 Thessaloniki, Greece
(Received 14 June 2000; revised manuscript received 14 March 2001; published 11 September 2001)

Carbon nitride (CN_x) films were deposited by reactive sputtering to study the effect of the ion bombardment during deposition (IBD) on their bonding structure. Fourier-transform infrared (IR) ellipsometry (FTIRE) was used to identify and distinguish the characteristic bands of the sp^3 C—N, sp^2 C═N, sp^1 (−C≡N, −N≡C) and the IR-inactive C═C bonds. The results are compared and discussed in view of the films' electronic behavior through the dielectric function $\varepsilon(\omega)$ in NIR-visible-UV region and with those obtained by nanoindentation measurements. The low-energy IBD is suggested to promote the homogeneous N distribution in the films, resulting in films with low hardness (~6 GPa) and stress. On the contrary, the high-energy IBD results in high-N concentration in localized regions of the films, where possibly the formation of fullerenelike and C_3N_4 structures is favored. Indeed, hardness values up to 45 GPa were measured at some regions of these films, along with the high stress and hardness that they exhibit. Their absorption due to $\pi \rightarrow \pi^*$ electronic transitions is higher and exhibit strong absorption ~1.6 eV where the low-energy IBD films are transparent. Furthermore, the effect of postdeposition thermal annealing to 900 °C on the bonding structure of the films was investigated. It was found that the structural modifications induced by the N removal from the carbon-nitrogen bonds depend on the bonding structure of the films, as determined by the IBD energy. The N evolution from sp^3 C—N bonds is more intense in low-energy IBD films and more pronounced around 450 °C, while the C—N bonds of pentagons and C_3N_4 structures, contained mainly in high-energy IBD films, are more stable and break at higher temperatures. Above 600 °C, N is evolved from the sp^2 C═N bonds, while the most stable structures (i.e., sp^1 −N≡C and −C≡N groups) break above 700 °C. The thermal treatment differentially affects the electronic transitions; the $\pi \rightarrow \pi^*$ are almost stable, while the strength and energy position of the $\sigma \rightarrow \sigma^*$ decrease. This reduction is dramatic in low-energy IBD films, suggesting an intensive N evolution from the sp^3- and sp^2-bonded nitrogen. The slight modification of $\varepsilon(\omega)$ and the unaffected film thickness at 900 °C reveal the high-thermal stability of high-energy IBD films. The above results indicate how IBD affects the bonding and electronic structure and the thermal stability of the CN_x films, contribute to the understanding of the bonding mechanisms during N incorporation in the *a*-C network, and provide insight towards the production of CN_x films with desired properties.

DOI: 10.1103/PhysRevB.64.125419 PACS number(s): 81.40.Tv, 82.80.Dx, 68.60.Dv

I. INTRODUCTION

Nitrogenated amorphous carbon materials have received considerable theoretical and experimental attention since Liu and Cohen predicted that the hypothetical material β-C_3N_4, structurally analogous to β-Si_3N_4, should have bulk modulus greater than that of a diamond.[1,2] Although a wide variety of techniques has been implemented,[3–9] there has been no clear evidence of the formation of crystalline stoichiometric β-C_3N_4, but only the existence of small crystallites of the β-C_3N_4 phase embedded in an amorphous carbon matrix is reported.[10–12] The difficulty to produce the β-C_3N_4 phase arises from the fact that the amount of N required to incorporate in the films is 57 at.%. However, CN_x films that are nitrogen deficient (~20–40 at.%), exhibit interesting properties such as high hardness and elasticity, comparable to other carbon-based materials. These properties have been attributed to a fullerenelike microstructure with curved basal planes that are cross linked through sp^3 coordinated bonds.[13–16]

Synthesis of carbon-nitride compounds has been attempted by a variety of techniques such as plasma-enhanced chemical vapor deposition (CVD),[5,8] ion-beam-assisted deposition[4,8] and laser ablation.[6,8] However, in spite of the great efforts to optimize the growth conditions, it is still difficult to understand the mechanisms responsible for the bonding structure in the CN_x films. Particularly among all the plasma-assisted techniques for synthesizing CN_x films, in rf magnetron sputtering, the growing film surface is subjected to a more intense ion bombardment as a consequence of the plasma sheath dynamics.[7,17] Although this mechanism significantly affects the bonding structure of the deposited films, a correlation between this mechanism and the distribution of N among the various bonding configurations with C has not been clearly established. This can be attributed to the absence of a detailed study where the different carbon-nitrogen bonding structures are accurately measured and clearly discriminated. Furthermore, although the thermal stability of the films is of considerable importance, there have been only a few thermal treatment studies of CN_x films. Post-deposition thermal annealing treatments are necessary for the identification of the stable phases and the determination of the films' thermal stability.

In this paper, we study the effect of the energy of the ion bombardment during deposition (IBD), which is controlled by the applied V_{bias}, on the bonding structure of reactively magnetron-sputtered CN_x thin films. Among the other experimental factors that affect the properties of the deposited films, the carbon-nitrogen bonding mechanisms are significantly affected by this ion bombardment during the films'

growth.[7,17] The *in situ* investigation of the vibrational properties of the films was performed using the Fourier-transform infrared (IR) ellipsometry (FTIRE) technique. FTIRE has recently emerged as a powerful optical technical for the accurate investigation of the vibrational properties of thin films. Its high sensitivity allows the identification of chemical bonds even in the cases of low-IR responses and it has the capability of the direct determination of the complex dielectric function that describes the material under study. Also, we report on the structural and compositional modifications of the films induced by post-deposition thermal treatment. Spectroscopic ellipsometry (SE) measurements in the NIR-Visible-UV spectral region (1.5–5.5 eV) were also performed in order to obtain information about the films' electronic structure and finally, nanoindentation and stress measurements to evaluate the hardness, elastic modulus, and stress of the films, respectively. It was shown that the IBD energy affects the N distribution in the films. Furthermore, the thermal treatment was found to modify the bonding structure of the films through the removal of N from carbon-nitrogen bonds followed by redistribution of N atoms to various bonding structures and by a subsequent N evolution from the films. Finally, the films' thermal stability has been correlated to their bonding structure as determined by the distribution of N atoms.

II. EXPERIMENTAL DETAILS

The CN_x films were deposited on *c*-Si(100) substrates by reactive rf magnetron sputtering using a graphite target of 99.999% purity in a deposition chamber with a base pressure better than 1×10^{-7} mbar. The substrates were located 65 mm above the target and coated using a sputtering power of 100 W. The sputtering gas was N_2 of 99.999% purity with a partial pressure of 4×10^{-3} mbar. The cleaning procedure of the substrates included chemical and ultrasonic cleaning before their introduction to the deposition chamber and etching with low-energy Ar^+ ion bombardment before deposition. The films were deposited at room temperature (RT), and each one by applying different V_{bias} on the substrate, ranging from -250 to $+16$ V (floating). The thicknesses of the films were $\sim$4500 Å.

The spectroscopic measurements were performed in the wave-number range from 900–3500 cm^{-1} at a resolution of 8 cm^{-1}, using a Fourier transform IR phase-modulated ellipsometer mounted through BaF_2 windows on the ultra high vacuum chamber by an angle of 70°. The IR beam is produced by a commercial IR spectrometer (BOMEM-MB100) which includes a thermal source of SiC bars and a Michelson interferometer. The IR beam is focused on the sample through an optical system of reflectors and lenses. A grid analyzer and a photo-elastic modulator, which modulates the IR beam polarization with a frequency of 37 kHz, define the polarization of the incident beam. After its reflection on the sample, the polarization of the IR beam is detected by a grid analyzer, and then is focused on the detection head through a suitable optical system. The detection head includes a HgCdTe (MCT) detector that covers the range of 900–4000 cm^{-1} and a InSb detector for the study in the range from 1800 to 4000 cm^{-1} with better sensitivity.

The partial pressures of the residual gases during the thermal treatment were monitored with a quadruple mass spectrometer (RGA). The films' electronic structure was investigated by SE measurements in the NIR-Visible-UV spectral region (1.5 to 5.5 eV) using a phase-modulated ellipsometer and finally, nanoindentation and stress measurements were used for the evaluation of the films' hardness, elastic modulus, and stress.

III. METHOD OF ANALYSIS

Ellipsometry, is a nondestructive technique that allows the *in situ* determination of the optical properties of the deposited films through the analysis of the complex reflectance ratio[18]

$$\rho = r_p / r_s , \tag{1}$$

where r_p and r_s are the Fresnel reflection coefficients for *p*- and *s*-polarized light that incidences at the planar interface between two semi-infinite optically isotropic media (0) and (1), with complex indices of refraction n_0 and n_1, respectively (two-phase model). The optical response of the medium (1) is determined by the complex dielectric function $\varepsilon(\omega)[=\varepsilon_1(\omega)+i\varepsilon_2(\omega)]$.

In the case of a film deposited on a substrate, we have the three-phase model where the film with thickness *d* [medium (1)] is confined between the semi-infinite ambient [medium (0)] and the substrate [medium (2)]. The complex reflectance ratio is defined as

$$\langle\rho\rangle = R_p / R_s , \tag{2}$$

where R_p and R_s are the Fresnel reflection coefficients. These depend on film thickness due to the multiple reflections of light between the media (0)–(1) and (1)–(2), through the phase angle (β) given by:

$$\beta = 2\pi(d/\lambda)(n_1^2 - n_0^2 \sin^2\theta)^{1/2}, \tag{3}$$

where λ is the wavelength, θ is the angle of incidence, and n_0, n_1 are the complex refraction indices of the ambient and the film, respectively. Thus, the measured quantity is the pseudodielectric function $\langle\varepsilon(\omega)\rangle[=\langle\varepsilon_1(\omega)\rangle+i\langle\varepsilon_2(\omega)\rangle]$ which also contains information about the substrate and the film thickness.

In the present paper, in order to minimize the contribution of the film thickness and the substrate on the measured spectra, all studied films have thicknesses around 4500 Å. As a result, the phase angle β diminishes in the energy region of high absorption, leading to $R_i = r_{01i} = r_i$, $(i=p,s)$ and consequently to $\langle\rho\rangle=\rho$. Thus, at the absorption bands, we only obtain information on the optical properties of the bulk of the film.

The vibrational properties of the films can be studied in the IR energy region, since the electric field of the IR beam causes the excitation of the bonding vibrations. These vibrations are modeled, to a first approximation, using a damped

harmonic oscillator (Lorentz model).[19–21] The effect of the several vibration modes on the complex dielectric function is described by the expression:

$$\tilde{\varepsilon}(\omega)=\varepsilon_\infty+\sum_i \frac{f_i\omega_{0i}^2}{\omega_{0i}^2-\omega^2+i\Gamma_i\omega}, \tag{4}$$

where ω is the energy of light and ω_{0i} is the absorption energy of the i^{th} vibration mode. The constants f_i and Γ_i denote the oscillator strength and the damping (broadening) of the specific vibration mode, respectively. The quantity ε_∞ that is described by the relation:

$$\varepsilon_\infty=1+\omega_p^2/\omega_0^2, \tag{5}$$

is the static dielectric constant and represents the contribution of the electronic transition that occurs at an energy ω_0 in the NIR-Visible-UV energy region, on the dielectric function.

In the case where more than one electronic transition occurs, their contribution is accounted by the summation $\Sigma_k[(\omega_{pk}^2)/(\omega_{0k}^2)]$. Thus, the contribution of the electronic transitions can be determined by studying ε_∞ out of the absorption bands. Furthermore, from Eq. (4) we can receive for $\omega=0$ that $\varepsilon_s=\tilde{\varepsilon}(\omega=0)=\varepsilon_\infty+\Sigma_i f_i$, where ε_s and $\Sigma_i f_i(\approx f_{\text{eff}})$ describes the losses in the material in the whole electromagnetic region and only in the IR region, respectively. Since the contribution of the various vibrational modes to the measured pseudodielectric function is weak, the calculation of the first derivative $d\langle\varepsilon\rangle/d\omega$ of the $\langle\varepsilon(\omega)\rangle$ allows the enhancement of the contribution of each structure around the absorption bands. The expressions of the real and imaginary parts of the first derivative of $\varepsilon(\omega)$ are:

$$\frac{d\varepsilon_1(\omega)}{d\omega}=-\sum_i \frac{2\,f_i\omega_{0i}^2\omega\cdot[\Gamma_i^2\omega_{0i}^2-(\omega_{0i}^2-\omega^2)^2]}{[(\omega_{0i}^2-\omega^2)^2+\Gamma_i^2\omega^2]^2}, \tag{6}$$

$$\frac{d\varepsilon_2(\omega)}{d\omega}=-\sum_i \frac{f_i\Gamma_i\omega_{0i}^2[(\omega_{0i}^2-\omega^2)(\omega_{0i}^2+3\omega^2)-\Gamma_i^2\omega^2]}{[(\omega_{0i}^2-\omega^2)^2+\Gamma_i^2\omega^2]^2}. \tag{7}$$

In order to obtain quantitative information from the measured IR spectra, we have performed two types of analysis. First, we analyzed the experimental data based on the Eqs. (2)–(4) assuming a layer of thickness d is deposited on a bulk substrate (c-Si). Thus, we obtain information about the films' bonding structure and the electronic properties, too. Second, we calculated the first derivative of the experimental spectra and we analyzed them by using Eqs. (6) and (7) assuming a bulk material around the region of the absorption bands. This analysis reveals information about the vibrational properties of the films. Combining the results from both analyses, as well as with those of the dielectric function in the NIR-Visible-UV spectral region, we obtain complete information about the bonding mechanisms, the electronic structure, and the microstructure of the films.

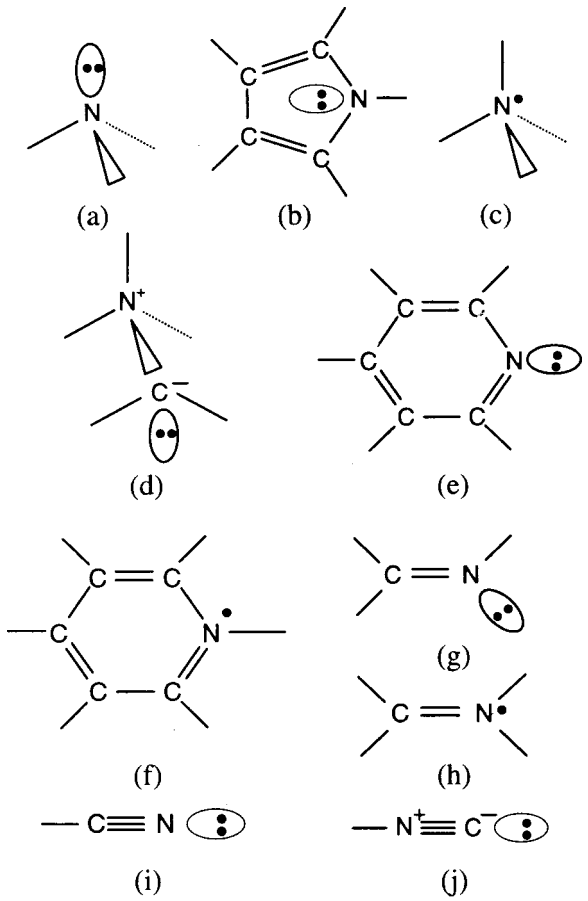

FIG. 1. Possible bonding configurations between N and C atoms: (a) to (d) sp^3 hybridized, (e), (f) N incorporated in aromatic rings, (g), (h) sp^2 hybridized (linear), (i) sp^1 hybridized nitrile group and (j) sp^1 hybridized iso-nitrile group.

IV. BONDING CONFIGURATIONS BETWEEN CARBON AND NITROGEN ATOMS

The study of the N incorporation into the a-C network has proven to be a complicated procedure since N has the ability to form with C several bonding configurations. These include the sp^3 (tetrahedral, C—N), sp^2 (trigonal, C═N) and the chain terminating sp^1 ($-$C≡N and $-$N≡C) bonds. Nitrogen has five valence electrons. These can be paired in σ, π bonds can be unpaired or also paired in a lone-pair orbital. In Fig. (1) the possible bonding configurations between N and C atoms are shown.[23]

The sp^3-hybridized carbon-nitrogen bonds are shown in Figs. 1(a)–1(d). In three-fold-coordinated substitutional sites, N atoms can form three σ bonds while the remaining two electrons form a lone pair [see Fig. 1(a)]. This stable configuration, found in Si_3N_4 is almost tetrahedral with a smaller bond angle (107.3°) than the bond angle of the tetrahedral structure (109.28°) since the electron lone pair takes up more space than the bonding electrons. This bonding configuration is found in pentagon rings [pyrrole-like structures, Fig. 1(b)], where the N atom is three-fold coordinated through two σ bonds, while a third σ bond can be formed. The remaining two electrons consist a lone-pair orbital, po-

TABLE I. Stretching vibration frequencies of the various bonding configurations.[a,b,c]

Group	Stretching vibration frequency (cm^{-1})
C—N (tetrahedral)	~1212−1270
C═N (graphitic ring)	~1530
C═N (chain)	~1650−1680
C═C	~1665−1680
−C≡N (terminating)	~2250
−N≡C (terminating)	~2150

[a]Reference 24.
[b]Reference 25.
[c]Reference 26.

sitioned perpendicularly to the pyrrole ring plane. In the tetrahedral structure [see Fig. 1(c)] the four of the five valence electrons from σ bonds and the last electron is unpaired. The bond angle of this structure is 109.28°. When the unpaired electron is transferred to another atom (first C neighbor) the N^+C^- defect group is formed [see Fig. 1(c)].

The ability of N atoms to form π bonds allows their incorporation into substitutional sites in six-membered graphitic rings [Figs. 1(e), 1(f) (pyridine-like structures)]. In the pyridine structure [see Fig. 1(e)], the N atoms forms two σ and one π bond, while the C atoms and the remaining two electrons form a lone pair located at the pyridine ring plane. If one of the lone-pair electrons is used for the formation of a σ bond [see Fig. 1(f)], the fifth electron remains unpaired in the antibonding π^* state. Other sp^2-hybridized bonding structures include the linear groups of Figs. 1(g), 1(h) with the N forming two and three σ bonds, respectively. In Figs. 1(i), 1(j) the sp^1 hybridized bonding structures are shown, which include the chain-terminating nitrile and the iso-nitrile groups. These structures are found to be relatively stable with high degrees of freedom. Since these bonding configurations saturate all the valence electrons of N, they induce the loss of connectiveness of the *a*-C network. This result to less densely packed structures. In Table I, the stretching vibration frequencies of the above mentioned bonding structures are given.

In addition, the vibration frequency of the pentagonal arrangements [Fig. 1(b)] coincides with the vibration frequency of the bonding structures where N atoms are sp^3 bonded to C. Also, the vibration frequency of each bonding structure depends on the atom species and the bonding configuration but also on its neighboring environment. Although the identification of bonding structures of different hybridization is possible, this is not the case for different bonding structures with the same hybridization state. The latter contribute to the FTIRE spectra in overlapping vibration bands that are difficult to distinguish.

V. EFFECT OF V_{bias} ON THE BONDING AND ELECTRONIC STRUCTURE OF CN_x FILMS

A. Vibrational analysis and assignment of bond configurations

The optical response of the CN_x films depends on the distribution of N atoms among the above-mentioned bonding

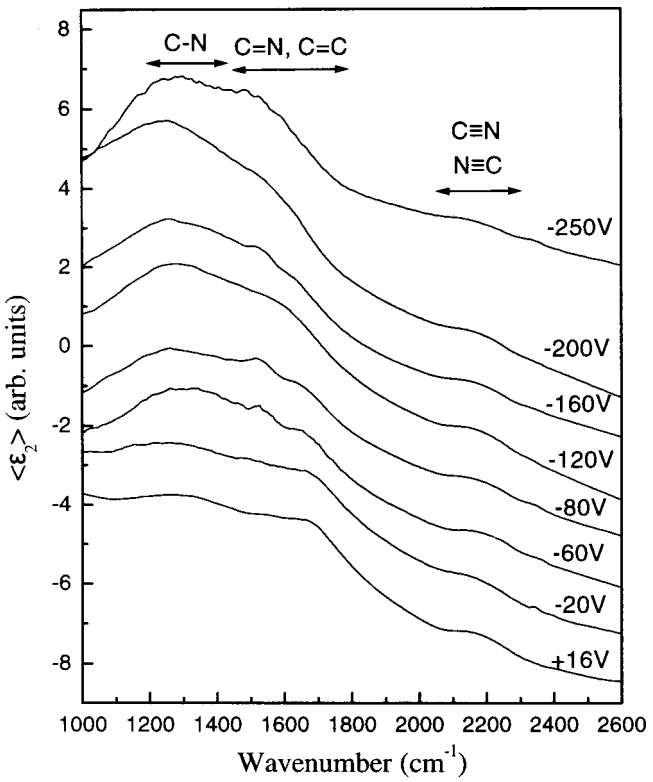

FIG. 2. Imaginary part of the pseudodielectric function spectra of the CN_x films for different values of V_{bias}.

configurations. The contribution of each oscillator to the measured pseudodielectric function is evidenced with a maximum in the imaginary part $\langle \varepsilon_2 \rangle$ together with an inflection in the real part $\langle \varepsilon_1 \rangle$. The study of the imaginary parts is preferable since the contribution of the vibrational modes is more pronounced in this representation.

In Fig. 2 the real and the imaginary part of the pseudodielectric functions of the CN_x films deposited with different V_{bias} is shown. Three characteristic bands can be distinguished. The broad band between 1200 and 1400 cm^{-1} is assigned to the stretching vibration of the C—N bonds,[24] and to the existence of pentagon rings [Fig. 1(b)] in the films. Finally, the characteristic band between 1400 and 1700 cm^{-1} is attributed to the stretching vibration of the sp^2 C═N and C═C bonds.[25] The weak shoulder between 2150 and 2250 cm^{-1} evidences the existence of the sp^1-hybridized nitrile (−C≡N) and isonitrile groups (−N≡C) in the films.[25]

The above differences in the IR response of the CN_x films are attributed to the IBD energy E_i, which is controlled by the applied V_{bias} onto the substrate through the relation $E_i = E_p + e|V_{bias}|$, where E_i is the discharge energy. Particularly, during the deposition of CN_x films with reactive magnetron sputtering, there exists an intense positive-ion bombardment on the growing film surface. The dominant positive ion species are the process gas ions N^+ and N_2^+ as well as sputtered carbon clusters C_n^+ and its reaction products with N, such as $(CN)_n^+$ and C_2N^+.[7,17] The flux and the energy of these species have a great effect in the mechanisms that govern the incorporation of N in the *a*-C network. V_{bias} increases the energy of the bombarding ions, enhancing the chemical

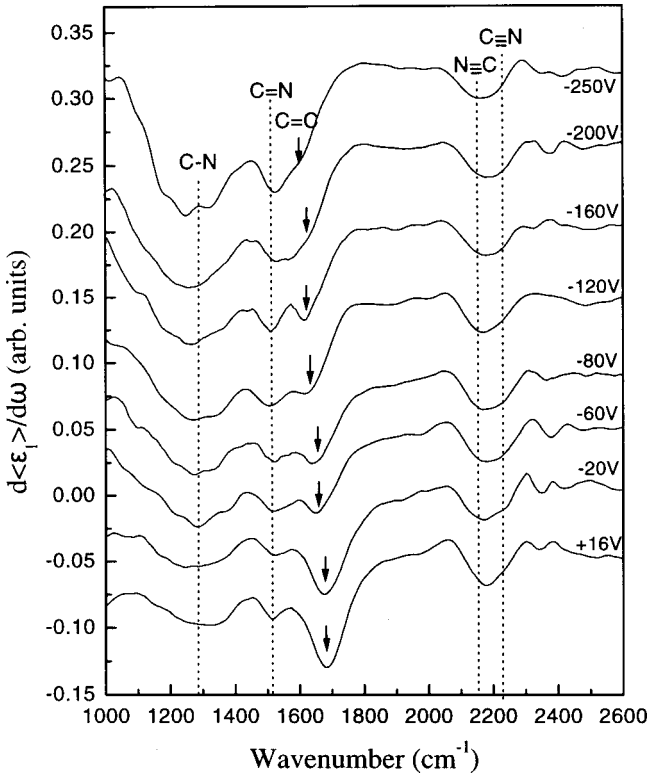

FIG. 3. First derivative of the real part of the measured pseudodielectric function $\langle\varepsilon(\omega)\rangle$ of CN_x films deposited with different V_{bias}. The dotted lines indicate the characteristic wave-number regions of the different bonding structures.

reactions between different species and their mobility at the growing film surface. As a result, the high-energy gas ions dissociate the sputtered carbon clusters affecting the N distribution, and thus, the bonding structure of the CN_x films.

Figure 3 shows the first derivative $d\langle\varepsilon_1(\omega)\rangle/d\omega$ of the real part of pseudodielectric function. The dotted lines indicate the characteristic bands corresponding to the various carbon-nitrogen bonding configurations. The differences in $d\langle\varepsilon_1\rangle/d\omega$ proves that the bonding structure of the CN_x films is significantly affected by the IBD energy. The characteristic band around 1300 cm^{-1} is attributed to the C—N bonds shown in Figs. 1(a)–1(d). The band at around 1530 cm^{-1} is assigned to the stretching vibration of the sp^2 C═N bonds contained in aromatic rings [see Figs. 1(e), 1(f)].[25] Since the stretching vibration frequency of the sp^2 C═N bonds contained in chains and C═C bonds is reported in the region from 1650 to 1680 cm^{-1}, and 1680 cm^{-1}, respectively, [25,26] their contribution is overlapped at the characteristic band at around 1680 cm^{-1} making difficult its separation. Thus, from this point below, we will consider both contributions. The C═C vibration mode is normally IR forbidden, since the C═C bond is a nonpolar bond. However, its contribution in the FTIRE spectra is the result of the N incorporation into the graphitic rings, which tends to destabilize the planar geometry of the rings, rendering the sp^2 C═C bonds IR active. [27] Also, the appearance of a small amount of the chain terminating nitrile (−C≡N) and iso-nitrile (−N≡C) groups is obvious in all spectra as a broad peak centered at about 2200 cm^{-1}.

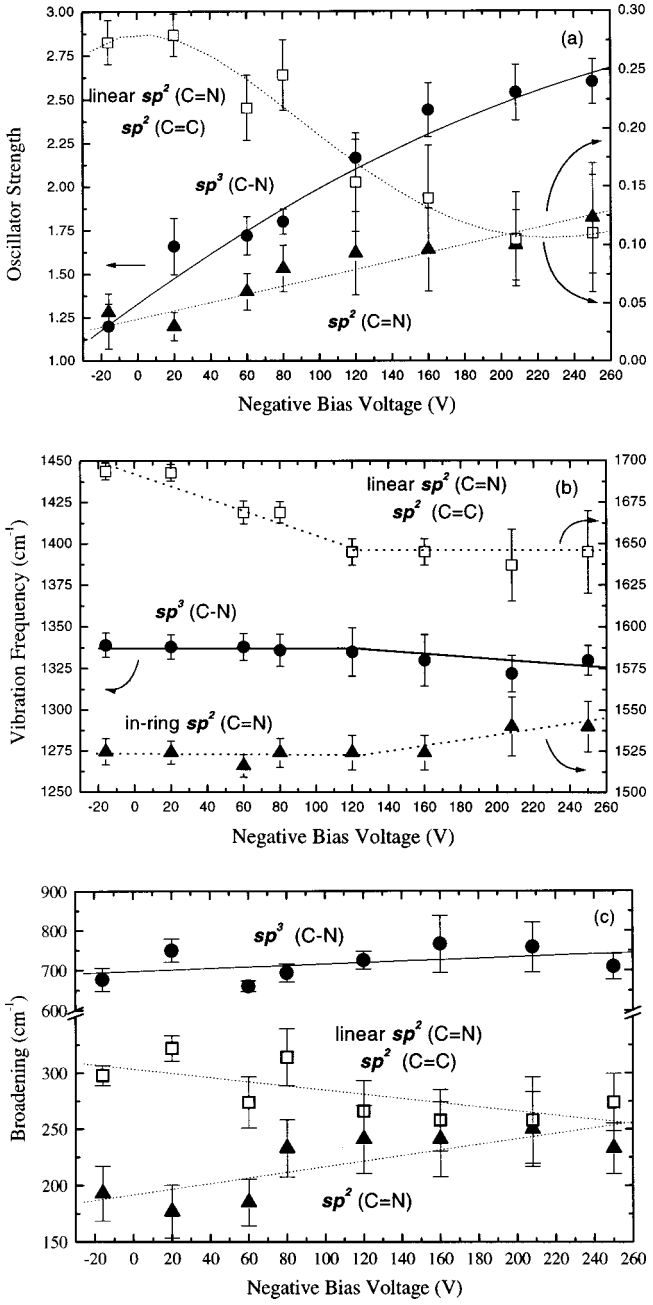

FIG. 4. Evolution of (a) oscillator strength, (b) vibration frequency, and (c) broadening of the sp^3 and sp^2 hybridized bonds with V_{bias}. The solid (dotted) lines are guides for the eye.

The vibration mode appeared at 2350 cm^{-1} is attributed to the presence of environmental CO_2 in the path of the IR beam outside the ultrahigh vacuum chamber. The evolution of the oscillator strength f, the vibration frequency, and broadening γ of different bonding configurations, as determined by analysis of the first derivative spectra using Eqs. (6) and (7), is plotted as a function of negative V_{bias} in Figs. 4, 5.

(i) sp^3 C—N bonds

The increase of the sp^3 C—N bond oscillator strength at films grown with high-negative V_{bias} and therefore high-

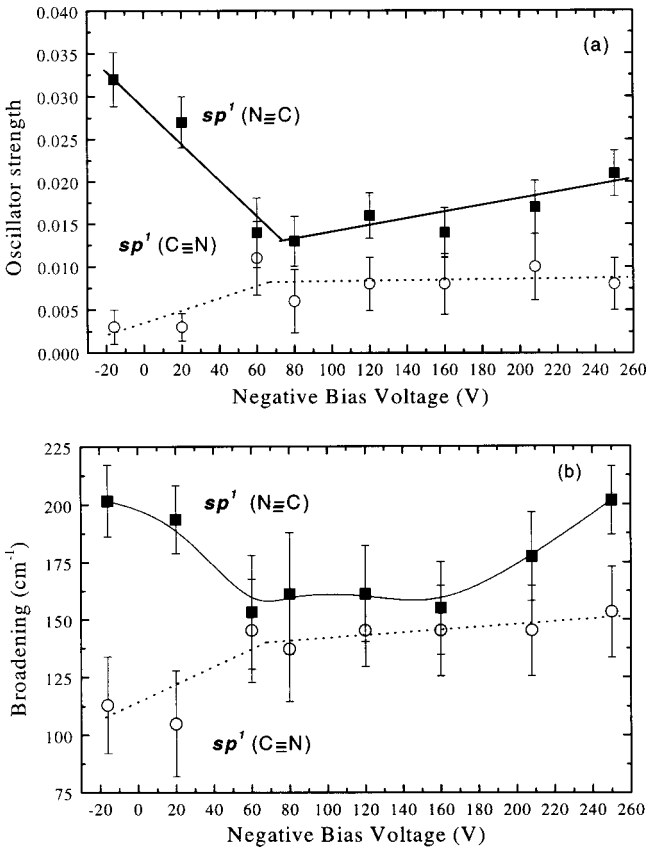

FIG. 5. Evolution of (a) oscillator strength and (b) broadening of the sp^1 hybridized bonds with V_{bias}. The solid (dotted) lines are guides for the eye.

energy IBD, indicates the favorable formation of these structures. Also, the stretching vibration frequency of the C—N bonds is initially constant, around 1338 cm^{-1} and reduces to ~1320 cm^{-1} for $|V_{bias}|>120$ V. This band represents the contribution of the tetrahedral C—N bonds contained either in pentagon rings [see Fig. 1(b)] or C_3N_4 structures. Thus, since the vibration frequency of the tetrahedral C—N bonds occurs at lower wave numbers [see Table I], it is suggested that at films grown with high-energy IBD, the formation of these structures is favored.

(ii) sp^2 C═N bonds in graphitic rings

The IR response of the sp^2 C═N bonds contained in graphitic rings is variable and very dependent on the local symmetry of the rings. The increase of these bonds at high-energy IBD films, as concluded by the increase of their oscillator strength, suggests that the graphitic rings contain a higher amount of N atoms. In addition, as seen in Fig. 4(b), the stretching vibration frequency of these structures starts to increase from 1525 up to 1540 cm^{-1} for $|V_{bias}|>120$ V.

(iii) Chain sp^2 C═N and sp^2 C═C bonds

The contributions of the chain sp^2 C═N bonds [see Figs. 1(g), 1(h)] and sp^2 C═C bonds are overlapped in the characteristic band between 1650 and 1690 cm^{-1}. The intense reduction of the oscillator strength at high-energy IBD films,

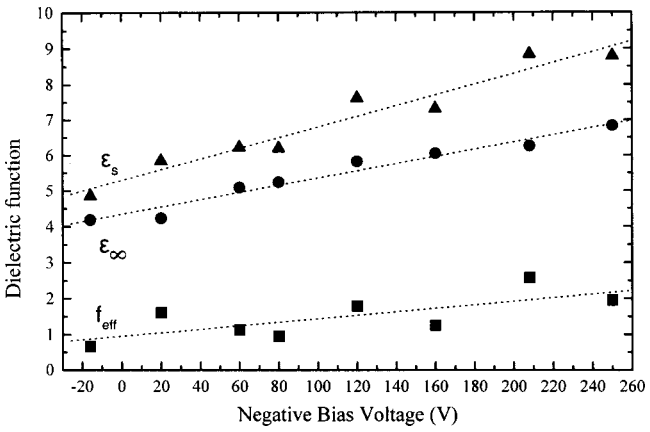

FIG. 6. Evolution of static dielectric constants and IR active bond contributions as a function on applied V_{bias}. The dotted lines are guides for the eye.

indicates the reduction of either one or both of these structures. Although it is difficult to separate each contribution and conclude about the effect of IBD energy on each bonding structure, the reduction of the stretching vibration frequency from 1690 to 1650 cm^{-1} for $|V_{bias}|>120$ V suggests that these structures are reduced at films grown with high-energy IBD. The reduction of the sp^2 C═C bonds could be the result of the existence of graphitic rings with more than one N atom because otherwise the distribution of N to a large number of rings induces a large-scale distortion to the graphite planar symmetry. The reduction of the band broadening γ, shown in Fig. 4(c), is in agreement with the above arguments.

(iv) sp^1 nitrile and iso-nitrile bonds

The stretching vibration frequency of the chain-terminating nitrile (−C≡N) and iso-nitrile (−N≡C) groups is found between 2210–2235 cm^{-1} and 2140–2170 cm^{-1}, respectively. Its variation with IBD energy is due to the different neighboring environment of these groups. The characteristic band of the iso-nitrile −N≡C group is generally broader than the bond of the nitrile −C≡N group, as shown in Fig. 5(c). However, the formation of these groups is gradually suppressed at high-energy IBD films. Since the existence of these structures causes the termination of the nitrogenated carbon network, their reduction results in the existence of densely packed structures that constitute a more tightly bound network.

B. Electronic structure of the CN_x films

Figure 6 shows the evolution of the static dielectric constants ε_s, ε_∞ and the IR-active bond contribution f_{eff} versus negative V_{bias} as determined by an analysis of the pseudodielectric function $\langle\varepsilon(\omega)\rangle$. The enhanced contribution of the various carbon-nitrogen bonds is confirmed by the increase of f_{eff} at high-negative V_{bias} and therefore, at high-energy IBD films.

According to Eq. (5), the increase of ε_∞, suggests that either the energy of the kth electronic transition ω_{0k} de-

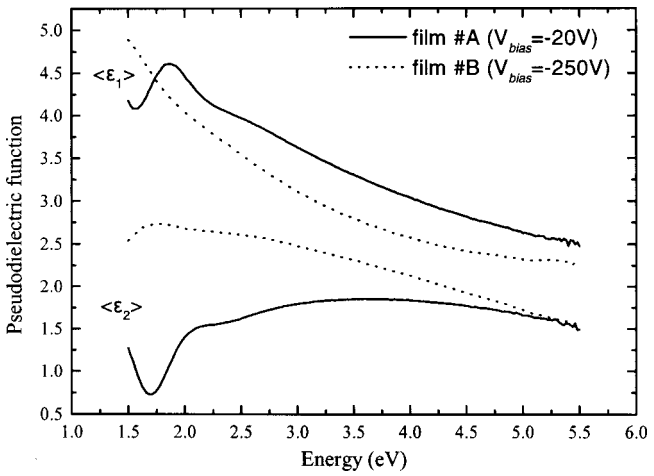

FIG. 7. Pseudodielectric function spectra in the energy region 1.5 to 5.5 eV of film #*A* and #*B*.

creases, or that the plasma energy ω_{pk}, which is analogous to density,[22] increases. This could also be explained by considering the Kramers-Kronig integrals

$$\varepsilon_1(\omega=0)=\varepsilon_\infty=1+\frac{1}{2\pi}\int_0^\infty \frac{\varepsilon_2(\omega')d\omega'}{\omega'}, \qquad (8)$$

where the static dielectric constant ε_∞ is conversely analogous to ω or analogous to $\varepsilon_2(\omega)$ (the density of states of electronic transitions) which is proportional to the films' density.

In order to understand how the variation of ε_∞ is correlated to the bonding structure of films grown with different IBD energy, their electronic properties were investigated by SE measurements in the NIR-visible-UV spectral region (1.5 to 5.5 eV). The results presented here involve two representative CN_x films grown with low-energy IBD ($V_{bias}=-20$ V, film #*A*) and high-energy IBD ($V_{bias}=-250$ V, film #*B*). Judging from the multiple reflections at 1.5–2.0 eV, it is obvious that film #*A* is more transparent than film #*B*. In general, the CN_x films can be treated as composite materials consisting of sp^2 and sp^3 coordinated carbon-carbon and carbon-nitrogen bonds while a low percentage of them can constitute sp^1 hybridized bonds. The latter because of their low polarizability, contribute slightly to the electronic dielectric function and possibly only at very high energies. Therefore, the sp^2 (C═C, C═N) and sp^3 (C—C, C—N) bonds are the main contributors to the electronic structure of the films and the existence of these bonds, as determined by the IBD energy is responsible for the observed variation in the measured $\langle\varepsilon(\omega)\rangle$.

Describing these bonds with the Lorentz oscillator dispersion relations and analyzing the $\langle\varepsilon(\omega)\rangle$ using the modified Tauc-Lorentz (TL) model[28] in combination with a three-phase (air/a-CN_x/*c*-Si) model,[18] it was found that the calculated ε_∞ values were in agreement with those determined by the FTIRE spectra analysis [see Fig. 6]. The fitting procedures were applied in the experimental spectroscopic ellipsometry (SE) spectra (Fig. 7), by taking into account two main electronic transitions (or oscillators) around 4 and 10 eV, in order to describe the dielectric response of the sp^2 and sp^3 sites. The dielectric function spectra for both films are shown in Fig. 8, in the energy region from 0 to 18 eV. These spectra were calculated using the parameters (oscillator energy, strength, and broadening), which were obtained by the best-fit procedure of the $\langle\varepsilon(\omega)\rangle$ and they are consistent with Kramers-Kronig integrals and sum rules. The position of the $\sigma\rightarrow\sigma^*$ electronic transitions, (attributed to both the sp^3 and sp^2 bonds),[29] is found at 11.7 (film #*A*) and 10.2 eV (film #*B*) whereas the one of the $\pi\rightarrow\pi^*$ electronic transitions (attributed only to sp^2 bonds) is found at 4.1 (film #*A*) and 3.77 eV (film #*B*). Due to the high-optical absorption of film #*B* at low energies, where appears a new structure, an additional oscillator at ~1.6 eV was needed for describing the measured pseudodielectric function. Although this structure has been correlated to the formation of a dense carbon phase,[30,31] it is not clear to us yet whether it is correlated to carbon-carbon and/or carbon/nitrogen bonds, too. The shift of both $\pi\rightarrow\pi^*$ and $\sigma\rightarrow\sigma^*$ electronic transitions to lower energies, their higher strength [higher $\varepsilon_2(\omega)$ values] and the existence of the transition at ~1.6 eV are the main differences in the electronic structure between films #*A* and #*B*. These contribute to the ε_∞ increase [see Eq. (8)] and they are the result of the increase of the IBD energy from film #*A* to #*B*.

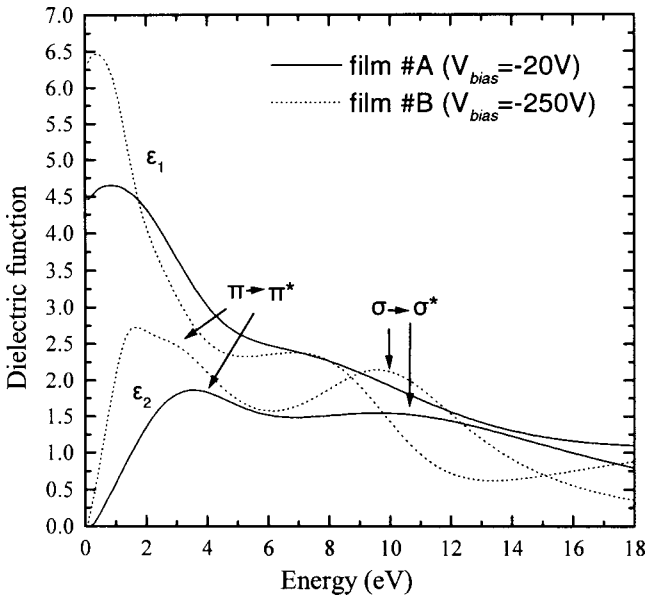

FIG. 8. Calculated $\varepsilon(\omega)$ spectra of film #*A* (solid lines) and #*B* (dotted lines).

The broadening of the $\sigma\rightarrow\sigma^*$ transitions in film #*B* is much smaller than in film #*A*, while the strengths of these transitions follow a different behavior between the two films. Therefore, in the case of film #*B*: (i) a less different type of bonds contribute to this transition and/or (ii) the bonds are characterized by well-defined bond lengths and angles. The former argument is supported by the lower contribution of the sp^2 (C═C, linear C═N) bonding structures in high-energy IBD films as determined by the FTIRE spectra analysis [see Fig. 4]. However, the higher strength of the $\pi\rightarrow\pi^*$ electronic transitions in film #*B* than in film #*A* is

consistent with the higher amount of in-ring sp^2 C═N bonds in films grown with high-energy IBD, as it was shown by the FTIRE spectra analysis.

C. Discussion

Theoretical investigations of the stability of graphite planes during the incorporation of N atoms randomly in substitutional C sites,[32] have revealed that as the [N]/[C] concentration increases from 0 to 1.0, the bands associated with σ and π electrons shift to larger binding energies, resulting in the increase of the $\pi \rightarrow \pi^*$ and $\sigma \rightarrow \sigma^*$ electronic transitions energies. However, these calculations are performed at specified bonding and crystallographic structures and it is difficult to be applied in the case of the CN_x films that contain several carbon-carbon and carbon-nitrogen bonding structures, which affect, in a preferential manner, the electronic structure of the films. Nevertheless, this argument is consistent to the calculated energy values of the $\pi \rightarrow \pi^*$ and $\sigma \rightarrow \sigma^*$ electronic transitions of films #*A* and #*B* and therefore indicates that N concentration is higher in film #*A*.

Indeed, representative x-ray photoelectron spectroscopy (XPS) measurements, not shown here, showed that the N concentration was slightly reduced from $35 \pm 5\%$ (low-energy IBD films) to $25 \pm 5\%$ (high-energy IBD films). However, this behavior cannot justify the significant differences in the bonding structure that high-energy IBD films exhibit. Thus, the observed IR response is mainly attributed to the distribution of N atoms in the films, as determined by the energy of the IBD controlled by the applied V_{bias}.

Therefore, the low-energy IBD (low-negative V_{bias}) results to a homogeneous N distribution in the films. Nitrogen is expected to occupy substitutional C sites through both sp^2 and sp^3 bonds in a large number of graphitic rings. This homogeneous N distribution results in the existence of a large amount of graphitic rings containing only one N atom, and consequently in a large-scale distortion of the graphite-plane symmetry.[13–15]

Theoretical investigations of the stability of the graphite planes upon substitution of C atoms with N,[32] have revealed that the increase of N concentration in the graphite planes above 20% results to the distortion of the planar symmetry. These distortions become more important at higher N concentrations. Although the CN_x films of the present work contain several carbon-carbon and carbon-nitrogen bonding structures apart from graphite rings, it can verify the validity of our results. The graphite ring distortion justifies the enhanced contribution of the sp^2 C═C vibration mode at 1680 cm^{-1} that low-energy IBD films exhibit.

The high-energy IBD (high-negative V_{bias}), promotes the increased concentration of N atoms in localized regions where a large amount of graphitic rings contain more than one N atom. This induces intense local distortions,[13–15] since the bond lengths of the C—N (1.47 Å) and C═N (1.22 Å) bonds are shorter than the lengths of C—C (1.54 Å) and C═C (1.33 Å) bonds contained in the graphitic rings. In order for these structures to relax, the formation of pentagon rings [see Fig. 1(b)] is expected. This transition from a planar to a corrugated structure, results in the local reduction of the distance between the basal planes (bending) and to the cross linking of the planes through sp^3 C—N bonds. The buckled basal planes, bonded with strong bonds, as three-dimensional structures enhance the mechanical properties of the films, since the covalent bonding is combined to a highly elastic behavior originated from the high degree of bond-angle deformation.[13–15]

Furthermore, the existence of a locally distorted network is expected to increase the internal stress of the films. Indeed, it was found that the compressive stress increases from 350 to 900 MPa at films grown from low-to high-energy IBD. Also, nanoindentation measurements, not shown here, indicate that films deposited with high-energy IBD, exhibit high hardness and are more capable of elastic recovery. Representative values of hardness H and elastic modulus E of these films are 12 and 140 GPa, respectively. The existence of three-dimensional structures at some high-energy IBD films is justified by hardness values up to ~45 GPa measured in some regions, as well as from x-ray diffraction (XRD) measurements,[33] which indicate the existence of C_3N_4 grains of 60–70 nm in these films. In contradiction with low energy IBD films that are characterized by low values of hardness ($H \sim 6$ GPa) and susceptibility to plastic deformation ($E \sim 75$ GPa).

VI. EFFECT OF THE THERMAL TREATMENT ON THE BONDING AND ELECTRONIC STRUCTURE OF CN_x FILMS

In order to verify the previous discussion concerning the assignment of the various characteristic bonds to the different carbon-nitrogen bonds and more importantly, to conclude about the thermal stability of the CN_x films, a thermal treatment from room temperature (RT) to 900 °C was employed. The thermal treatment modifies the microstructure of the CN_x films through: (i) break of the carbon-nitrogen bonds,[34,35] (ii) N redistribution between the possible bonding configurations with C atoms, and (iii) evolution of C (through oxidation) and N atoms from the films. The present paper involves the above-described representative CN_x films #*A* and #*B*. The FTIRE spectra were obtained before the annealing treatment and at RT after annealing to various temperatures.

A. Vibrational analysis

The effect of the thermal treatment on the bonding structure of the films, is shown in Fig. 9. The contribution of the vibration modes of the sp^3, sp^2, and sp^1 bonds to the pseudodielectric function reduces at higher temperatures, but not similarly in both films. This modification is a direct result of the N evolution from carbon-nitrogen bonds. The characteristic bands corresponding to the various carbon-nitrogen bonds appear more narrow and localized at certain limits. This can be explained by considering that each type of carbon-nitrogen bond exhibit certain variations in the bond lengths and angles induced by their neighboring environment. Therefore, at the first stages of the thermal treatment, N is preferentially removed from the most volatile bonds

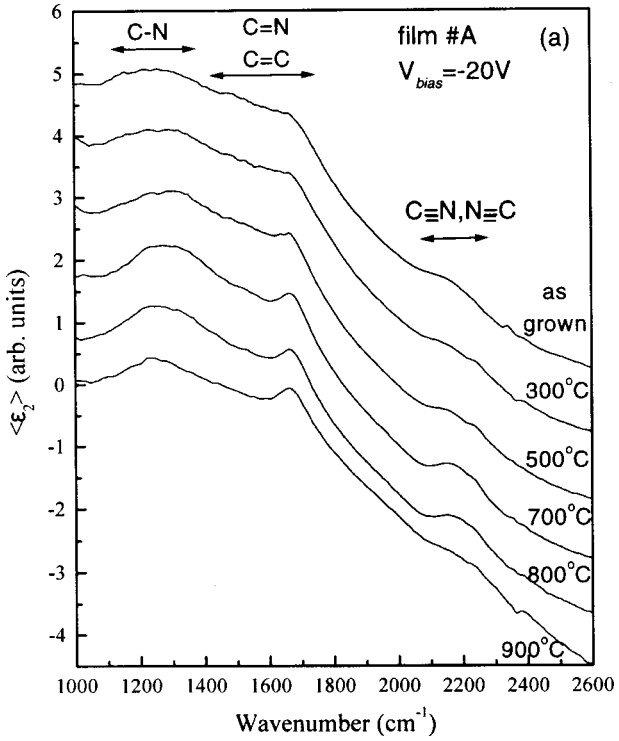

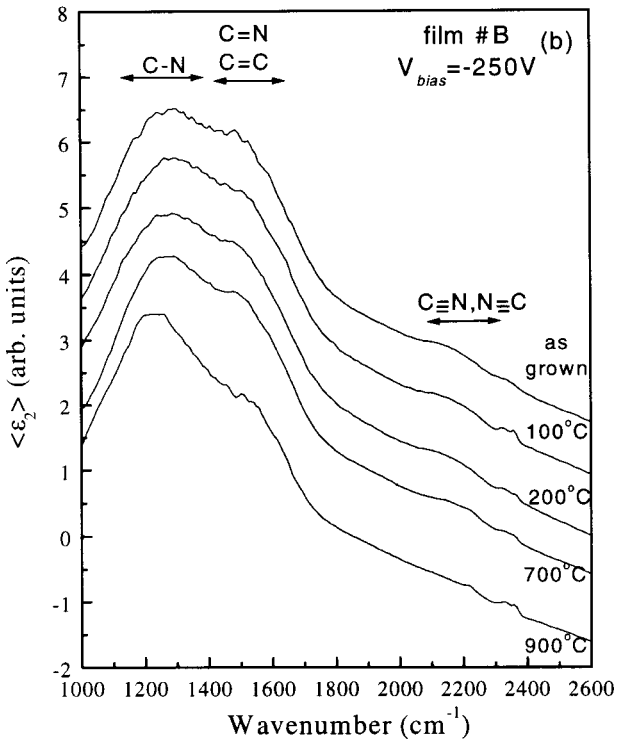

FIG. 9. Imaginary part of the pseudodielectric function of films (a) #*A* and (b) #*B*, as grown and annealed to various temperatures.

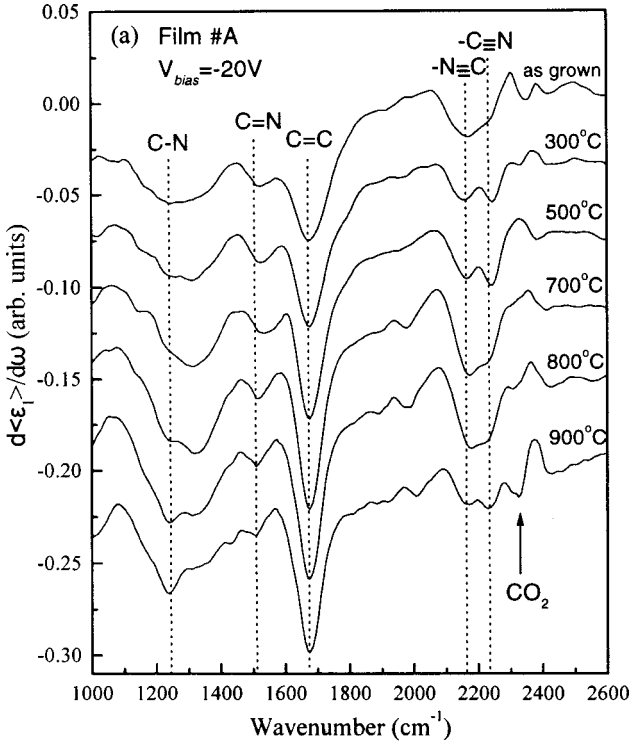

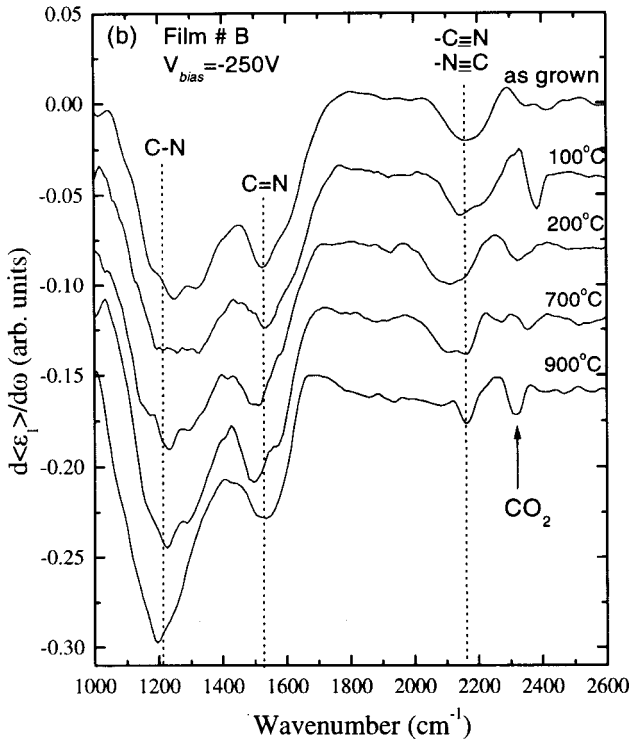

FIG. 10. First derivative of the real part of the pseudodielectric function of (a) film #*A* and (b) film #*B* as grown and annealed to various temperatures.

with large variations in bond lengths and angles, while the pure bonding structures appear more resistant.

(i) sp^3 C—N bonds

The stretching vibration frequency [see Figs. 10 and 11] reduces at higher temperatures in both films. Particularly, in film #*A*, it is almost constant and above 600 °C it reduces from 1340 to 1320 cm^{-1} because at the initial stages of the thermal treatment, N is preferentially evolved from bonding structures with large variations in lengths and angles shifting the stretching vibration frequency to 1300 cm^{-1}. This behav-

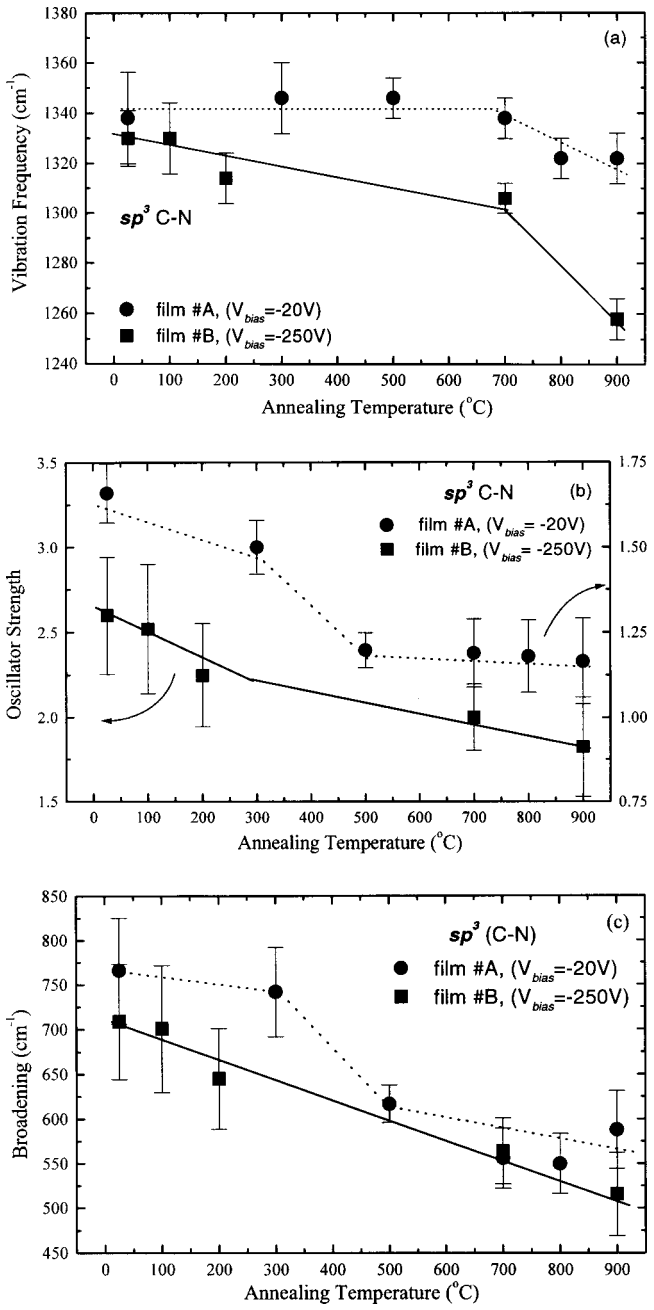

FIG. 11. Variation of (a) vibration frequency, (b) oscillator strength, and (c) broadening of the sp^3 hybridized C—N bonds with the annealing temperature of films #*A* and #*B*. The solid (dotted lines) are guides for the eye.

ior is more intense in film #*B* since a gradual decrease from 1330 cm^{-1} at RT, to 1258 cm^{-1} at 900 °C is observed. Thus, the contribution of fullerenelike (through the existence of pentagon rings) and possibly C_3N_4 structures, is more pronounced in the FTIRE spectra of film #*B* after annealing to temperatures above 600 °C. That is, since the characteristic vibration frequencies of these structures is reported between 1212–1270 cm^{-1}. At higher temperatures, N evolution from pentagon rings is more intense. In accordance with the behavior of the oscillator strength and broadening, the break of C—N bonds is more intense in film #*A* at temperatures between 350 and 500 °C.

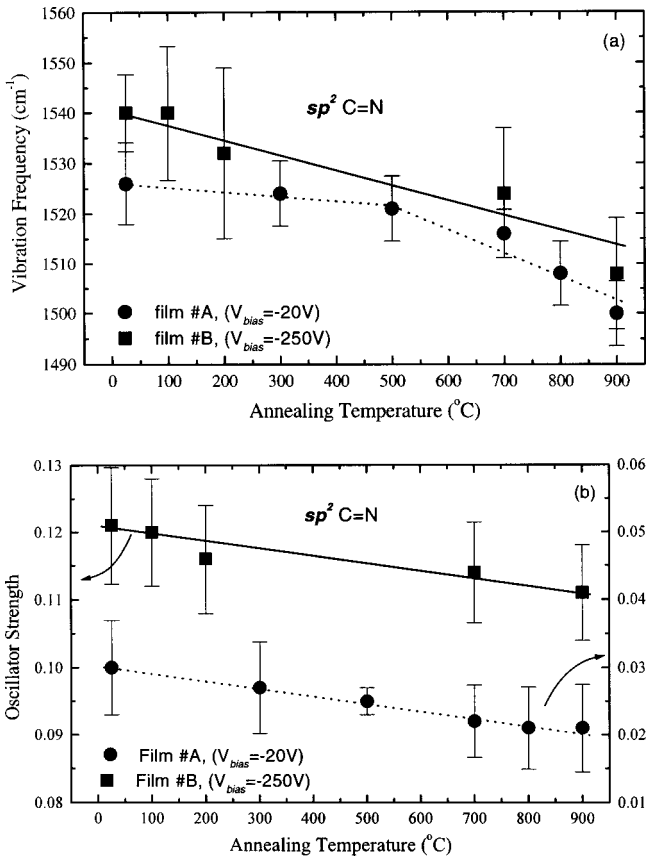

FIG. 12. Variation of (a) vibration frequency and (b) oscillator strength of the sp^2 hybridized C═N bonds with the annealing temperature of films #*A* and #*B*. The solid (dotted) lines are guides for the eye.

(ii) sp^2 C═N bonds in graphitic rings

The vibration frequency of the in-ring sp^2 C═N bonds reduces with temperature from 1525 cm^{-1} at RT to 1496 cm^{-1} at 900 °C (film #*A*) and from 1540 cm^{-1}at RT to 1510 cm^{-1} at 900 °C (film #*B*) as shown in Fig. 12(a). Particularly, this reduction in film #*A* is more intense above 600 °C. This, in combination with the gradual decrease of the oscillator strength [see Fig. 12(b)], suggests that N must be removed from sp^2 C═N bonds with continuously smaller variations in lengths and angles.

(iii) Linear sp^2 C═N and sp^2 C═C bonds

Figure 13(a) shows that the stretching vibration frequency of the characteristic band corresponding to sp^2 C═C and linear C═N bonds reduces from 1690 cm^{-1} RT to 1682 cm^{-1} (900 °C) and from 1645 (RT) to 1600 cm^{-1} (900 °C) at films #*A* and #*B*, respectively.

In the case of film #*A*, this reduction in combination with the observed increase of the oscillator strength [see Fig. 14(b)] implies that the thermal annealing promotes the redistribution of evoluted N atoms to various sp^2 bonding configurations. This also results in the increased contribution of sp^2 C═C bonds. Film #*B* exhibits a similar behavior, however, the reduction of the stretching vibration frequency from 1645 to 1600 cm^{-1} at 900 °C suggests an increased amount

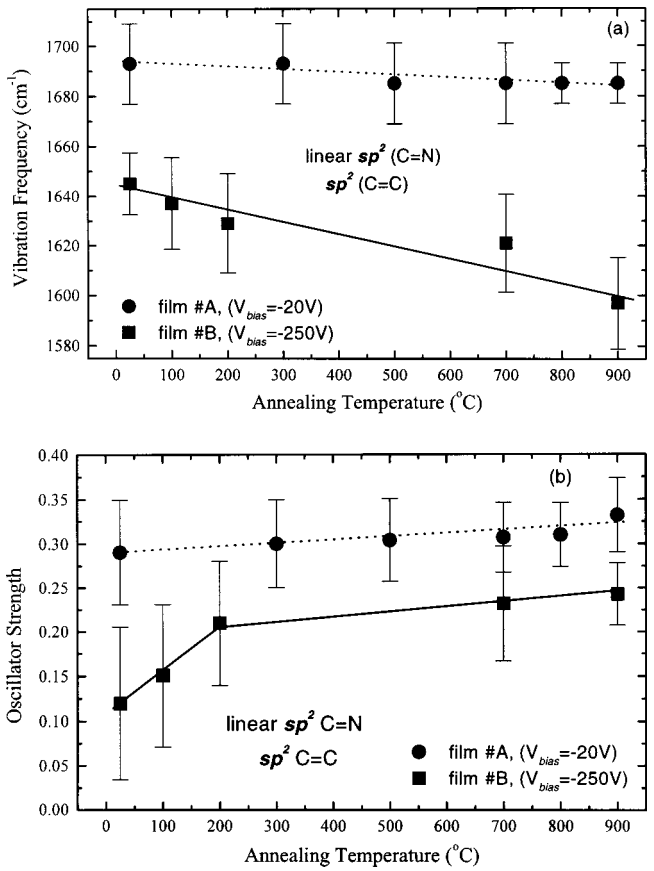

FIG. 13. Variation oscillator strength of the sp^1 hybridized nitrile ($-$C≡N) and iso-nitrile ($-$N≡C) bonds with the annealing temperature of films #*A* and #*B*. The solid (dotted) lines are guides for the eye.

of IR-active C═C bonds attributed either to the intense redistribution of the evoluted N to different sp^2 bonding structures in the films and or to the increase of sp^2 C═C bonds in the film.

(iv) sp^1 nitrile and iso-nitrile bonds

The stretching vibration frequency of the chain terminating sp^1 nitrile ($-$C≡N) and iso-nitrile ($-$N≡C) groups was found to be unaffected by the thermal treatment. The amount of the iso-nitrile ($-$N≡C) bonds remains almost stable until 700 °C, in both films, where these structures start to break. In contrary, the amount of the nitrile ($-$C≡N) bonds increases in film #*A* throughout the thermal treatment, while in film #*B*, is significantly reduced. Since this terminating type of bonding induces the loss of connectiveness of the *a*-C network, its increase during the thermal treatment suggests that film #*A* becomes less tightly bound and becomes even more unstable. In contrary, the reduction of the amount of these structures in film #*B*, suggests a more dense film structure at higher temperatures contributing to the films thermal stability.

C. Electronic structure of the annealed CN_x films

Figure 17 shows the evolution of the static dielectric constant $\varepsilon_s, \varepsilon_\infty$ and the overall contribution f_{eff} of the IR-active

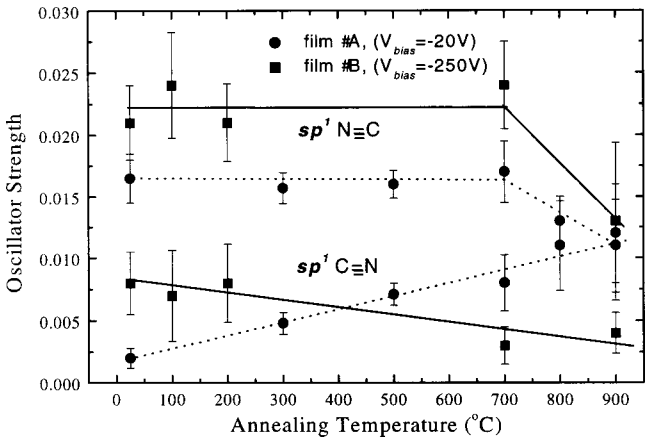

FIG. 14. Variation of (a) vibration frequency and (b) oscillator strength of the linear sp^2 C═N and sp^2 C═C bonds with the annealing temperature of films #*A* and #*B*. The solid (dotted) lines are guides for the eye.

bond, of films #*A* and #*B*, at RT and after annealing to various temperatures up to 900 °C. The removal of N from the carbon-nitrogen bonds is responsible for the observed reduction of f_{eff} whereas the reduction of ε_∞ can be attributed to (a) the shift of the electronic transitions to higher

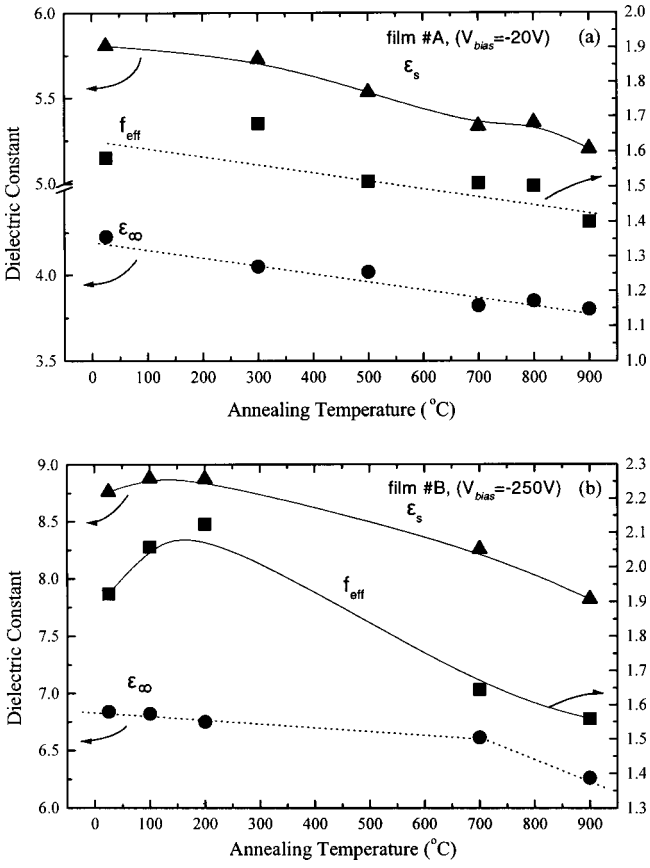

FIG. 15. Variation of static dielectric constants and IR active bond contributions as a function of the annealing temperature for (a) film #*A* and (b) film #*B*. The solid (dotted) lines are guides for the eye.

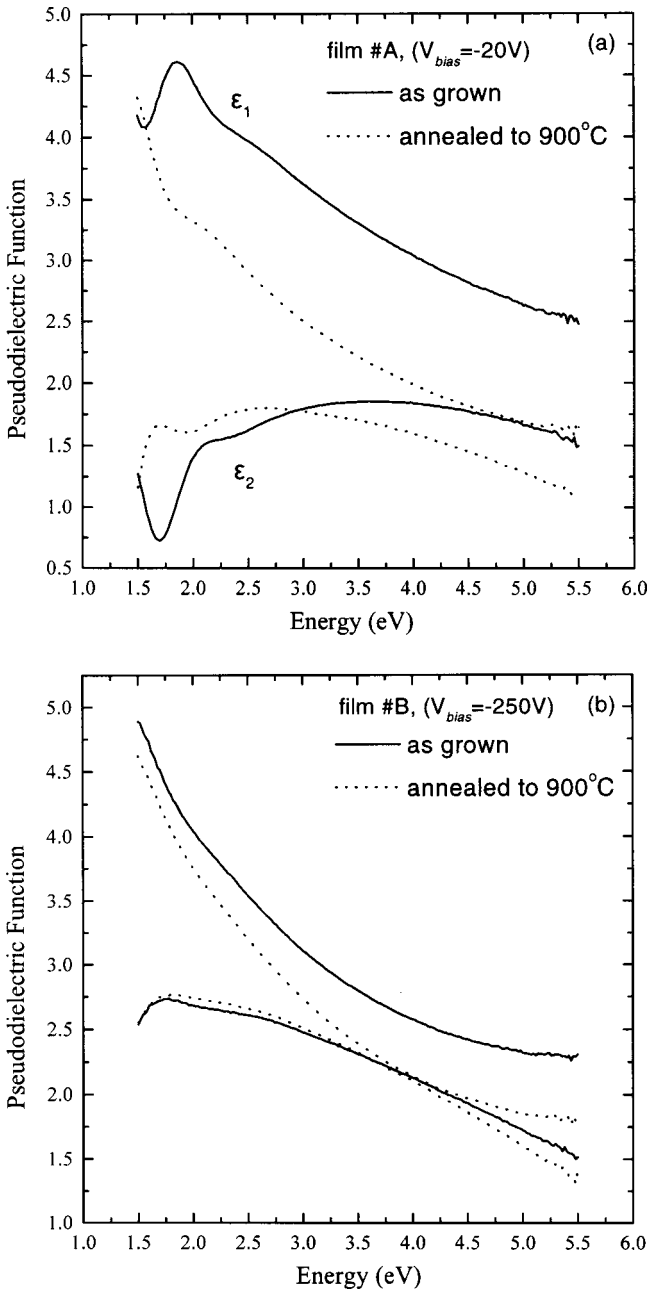

FIG. 16. Pseudodielectric function spectra in the 1.5–5.5 eV energy region for (a) film #*A* and (b) film #*B*, as grown (solid line) and annealed to 900 °C (dotted line).

energies, (b) their strength reduction (bonds break), and (c) the formation of microvoids in the films. The latter, however, we expect to contribute less, due to the densification induced by the temperature.

From Fig. 15(a) it is clear that the variation of f_{eff} and ε_∞ are correlated, suggesting that N is evoluted from bonding structures that contribute to the film's electronic behavior. Although this behavior is also shown in Fig. 15(b) (film #*B*), at low temperatures a direct correlation between f_{eff} and ε_∞ cannot be established. This could be explained by considering that at low temperatures the evolution of N atoms must be followed by a certain redistribution of N between different bonds with C atoms. Another possible explanation could be that the additional oscillator at ~1.6 eV that strongly affects ε_∞ is not correlated to a carbon-nitrogen bonding and therefore does not contribute to the IR response. In order to get more insight, we studied the films' measured pseudodielectric function, as grown and annealed to 900 °C, in the energy region 1.5–5.5 eV [Fig. 16]. Although $\langle \varepsilon_1(\omega) \rangle$ is dramatically reduced in film #*A*, this reduction is not followed by a similar one in $\langle \varepsilon_2(\omega) \rangle$, indicating a reduction of the strength of the electronic transitions in the high-energy region, where $\sigma \rightarrow \sigma^*$ transitions take place. The thermal treatment has not induced significant modifications in the electronic structure of film #*B* since a similar, yet not so pronounced behavior, is also observed.

The calculated $\varepsilon(\omega)$ spectra[18,28] before and after the thermal treatment of the CN_x films are shown in Fig. 17. The calculated energies of the $\pi \rightarrow \pi^*$ and $\sigma \rightarrow \sigma^*$ electronic transitions in both films are summarized in Table II.

The $\pi \rightarrow \pi^*$ electronic transitions energy of film #*A* (see Table II) is reduced from 4.1 eV (RT) to 3.5 eV (900 °C), while the $\sigma \rightarrow \sigma^*$ transitions energy is significantly reduced from 11.7 eV (RT) to 8.5 eV (900 °C). This behavior is accompanied by a small reduction of the $\pi \rightarrow \pi^*$ transitions strength and a dramatic reduction of the $\sigma \rightarrow \sigma^*$ one. At this point, we should note that the observed electronic transitions contain the overall contributions of different bonding structures. For example, the $\sigma \rightarrow \sigma^*$ electronic transitions include the individual contribution of both sp^2 (C═N,C═C) and sp^3 (C—N,C—C) bonds.[29,36]

Therefore, the intense reduction of the $\sigma \rightarrow \sigma^*$ electronic transitions strength and energy position can be attributed to the N and C evolution (see below) from both sp^2 and sp^3 bonds. The slight reduction of the $\pi \rightarrow \pi^*$ transitions strength could be the overall effect of (a) the reduction of the sp^2 C═N bonds, (b) the redistribution of a part of the evoluted N to sp^2 bonded structures, and (c) the increase of sp^2 C═C bonds. The latter was also concluded by the FTIRE spectra analysis [Fig. 14(b)].

The electronic structure of film #*B*, as determined by the $\varepsilon(\omega)$, is affected much less by the thermal treatment. In particular, the strength and energy (3.77 eV at RT to 3.79 eV at 900 °C) of the $\pi \rightarrow \pi^*$ electronic transitions are almost constant. This indicates that either a part of the evoluted N in film #*B* is redistributed and rebonded as sp^2 (C═N) or the amount of the sp^2 C═C bonds is increased due to the N removal from the film.

The $\sigma \rightarrow \sigma^*$ transitions energy shifts to higher energies, opposite to what is found in film #*A*. This, in combination to the slight reduction of their strength, justifies the redistribution between sp^3 and sp^2 bonded structures. The strength of the electronic transition located at the lower energies is significantly reduced and is shifted from 1.6 eV (RT) to 1.7 eV (900 °C). Although this structure has been correlated to a dense carbon phase,[30,31] it is not clear whether or not it is correlated only to carbon-carbon or to carbon-nitrogen bonding structures. We note, however, that this structure contributes significantly to the ε_∞ reduction. Finally, from the study of IR response of film #*B* and the small modifications in its electronic structure or the $\varepsilon(\omega)$, induced by the thermal treat-

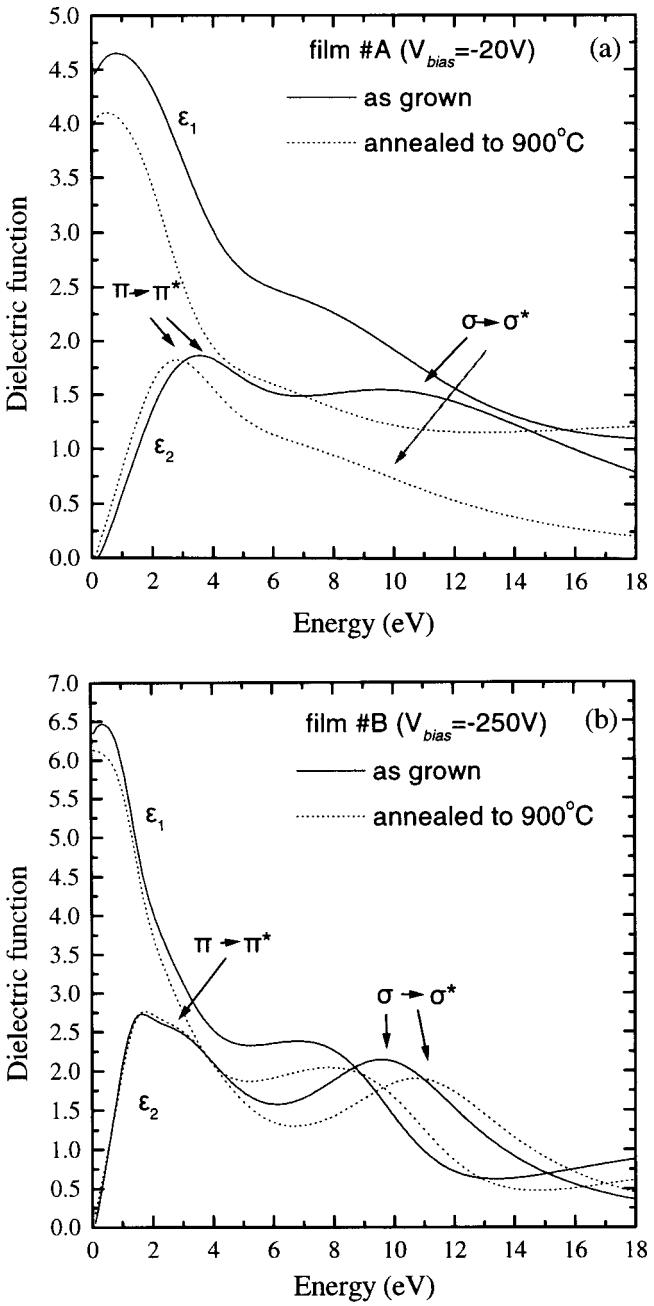

FIG. 17. Simulated $\varepsilon(\omega)$ spectra of (a) film #*A* and (b) film #*B*, as grown (solid line) and annealed to 900 °C (dotted line).

ment, we are drawn to the conclusion that the high-energy IBD leads to the production of thermally stable films.

In addition, from x-ray reflectivity measurements we have found that films #*A* and #*B* have densities $\rho=1.75$ and $\rho=2.05\,\mathrm{g/cm^3}$, respectively. The higher density of the high-energy IBD films is correlated to the higher amount of sp^3 sites and to the lower amount of voids, as defined by the N distribution in the amorphous carbon network. Therefore, the N evolution and the structural rearrangements, induced by the thermal treatment, are the direct result of the films' bonding structure.

TABLE II. Electronic transitions energies of CN_x films before and after annealing to 900 °C.

	$\pi\rightarrow\pi^*$ electronic transition energy (eV)		$\sigma\rightarrow\sigma^*$ electronic transition energy (eV)	
	RT	900 °C	RT	900 °C
Film #*A*	4.1±0.1	3.5±0.2	11.7±0.8	8.5±0.8
Film #*B*	3.77±0.2	3.79±0.1	10.2±0.9	11.4±0.9

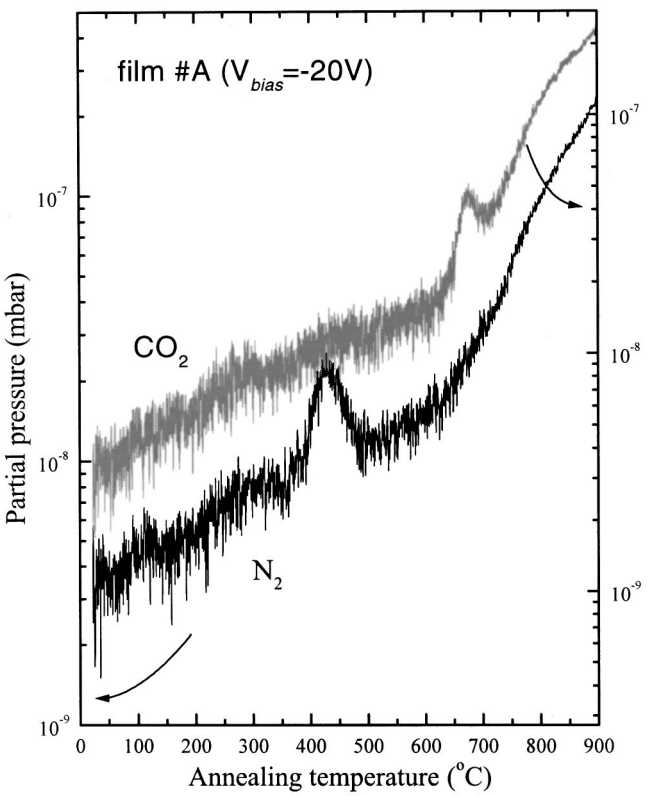

FIG. 18. Evolution of N_2 and CO_2 partial pressures during the thermal treatment of film #*A* from RT to 900 °C.

The variation of the films' thickness during the thermal treatment can further confirm their thermal stability, since it is associated with the induced structural and compositional modifications of the films. Indeed, from the FTIRE spectra analysis, it was found that the thickness of the high-energy IBD film (#*B*) was substantially unaffected, even at 900 °C. In contrary, although at temperatures up to 700 °C the thickness of the low-energy IBD film (#*A*) was stable, above 700 °C and up to 900 °C decreased ~10%. This reduction is attributed not only to the N removal from the various carbon-nitrogen bonds but also to the C atom evolution from the film through oxidation.

Verification for the above arguments arises from the study of the partial pressures of the residual gases in the deposition chamber monitored during the thermal treatment of film #*A*. The partial pressures of N_2 and CO_2 denoted as $P(N_2)$ and $P(CO_2)$, respectively, is shown in Fig. 18 and is a direct measure of N and C atom evolution from the films. The evolution of $P(N_2)$ starts from the initial stages of the thermal treatment and it increases intensively after 370 °C. This behavior is indicative of the N removal mainly from C—N bonds and it confirms the reduction of the C—N bond oscil-

lator strength, [Figs. 11(b)]. At around 450 °C, this behavior starts to saturate while at ~520 °C, $P(N_2)$ is reduced dramatically, since the amount of N contained in graphitic rings [see Figs. 1(e), 1(f)] has significantly reduced. The N atom removal preferentially from continuously more stable bonding structures, proceeds as temperature increases above ~520 °C. Furthermore, the N atom removal from sp^2 C═N bonds is also dominant at these temperatures, since at lower temperatures the break is facilitated for the more volatile C═N bonds with relatively large variations in bond lengths and angles. The $P(CO_2)$ evolution follows the same behavior as $P(N_2)$ suggesting that the removal of N from carbon-nitrogen bonds induces C evolution through oxidation. The sharp increase of $P(N_2)$ above 650°C reveals the evolution of N even from the most stable bonding structures such as the chain terminating sp^1 nitrile ($-$C≡N) and iso-nitrile ($-$N≡C) groups as it is also shown from the results of the FTIRE spectra analysis (Fig. 15). This sharp increase is followed by a similar one in $P(CO_2)$ suggesting that the evolution of C from the film is more intense at these temperatures, justifying the thickness reduction. It should be noted that the partial pressures of the other species monitored (N,O,O_2,C,CN,CN_2, etc.) were below 1×10^{-8} mbar and showed no significant changes during annealing.

IV. SUMMARY AND CONCLUSIONS

Carbon-nitride films have been synthesized by reactive magnetron sputtering on *c*-Si substrates biased with voltages in the range from -250 to $+16$ V in order to study the effect of the IBD on their bonding and electronic structure. Also, the structural modifications induced by post-deposition thermal annealing to 900 °C were studied. The concluding remarks are summarized in the following.

(i) The characteristic bands of the sp^3 C—N, sp^2 C═N, and sp^1($-$C≡N,$-$N≡C) bonds were identified and distinguished at around 1300, 1530, and 2200 cm^{-1}, respectively. Also, a characteristic band between 1650 and 1690 cm^{-1} revealed the contribution of the linear sp^2 C═N and the normally IR-inactive sp^2 C═C bonds. The appearance of the latter to the FTIRE spectra was the result of the distortion of the graphitic ring symmetry. Since the N concentration in the films does not vary much, the observed differences in their bonding and electronic structure is the result of the N bonding and distribution as affected by the IBD energy controlled by the applied V_{bias}.

(ii) The low-energy IBD promotes the homogeneous N distribution in the films and in a large number of graphitic rings containing one N atom and resulting in a large-scale distortion of the graphite plane symmetry. This is confirmed by the enhanced contribution of the sp^2 C═C bonds, which are normally IR inactive, to the FTIRE spectra. Also, the existence of a large amount of linear sp^2 C═N bonds at these films is evidenced by the characteristic band around 1680 cm^{-1}.

(iii) The high-energy IBD promotes the nonhomogeneous N distribution in localized regions in which the graphitic rings possibly contain more than one N atom (at these regions the amount of N can be above the average one measured in the films). This results to a local concentration of sp^3 C—N and sp^2 C═N bonds and to an intense local distortion of the graphitic planar geometry. At these regions, three-dimensional bonding structures are formed either through the bending and crosslinking of the basal planes with sp^3 coordinated bonds,[13–15] or through the formation of C_3N_4 structures. Indeed, high-energy IBD films are found to exhibit, at some regions, hardness values ~45 GPa indicating a combination of covalent bonding and a high degree of bond-angle deformation, and the existence of C_3N_4 grains ~70 nm.

(v) SE measurements in the energy region 1.5–5.5 eV revealed several differences in the electronic structure between low- and high-energy IBD films, associated mainly to the $\pi\rightarrow\pi^*$ and $\sigma\rightarrow\sigma^*$ electronic transitions. The high-energy IBD results to an energy shift of both $\pi\rightarrow\pi^*$ and $\sigma\rightarrow\sigma^*$ electronic transitions to lower energies, an increase of their strength and an increase of the static dielectric constant ε_∞. In addition, these films exhibit a transition at ~1.6 eV. It is not clear however, whether this is related to carbon-carbon and/or to carbon-nitrogen bonds.

(vi) The post-deposition thermal treatment results to an intense N atom evolution from various carbon-nitrogen bonding structures, especially from the low-energy IBD films. Particularly, the break of sp^3C—N bonds is more pronounced between 370 and 520 °C, reaching saturation at ~450 °C. However, in the case of high-energy IBD film, the nitrogen incorporated in pentagon rings and C_3N_4 structures was suggested to break at higher temperatures, as the shift of the sp^3 C—N bond vibration frequency to lower wave numbers indicates. Above 600 °C nitrogen is removed also from sp^2 C═N bonds, while a part of it is redistributed to various sp^2 bonding structures. Finally, above 700 °C N atoms are evoluted from the most stable bonding structures, such as the chain terminating sp^1 nitrile ($-$C≡N) and iso-nitrile ($-$N≡C) bonds. By comparing the variation of the oscillator parameters corresponding to the various carbon-nitrogen bonds, we are drawn to the conclusion that higher-thermal stability characterizes the high-energy IBD films.

(vii) The $\varepsilon(\omega)$ in the NIR-Visible-UV spectral region was less affected by the thermal treatment in high-energy IBD film, confirming its higher-thermal stability. This is also confirmed by its thickness stability at high temperatures. In contradiction, the thickness of the low-energy IBD film reduces significantly above 700 °C due to the intensive removal of C atoms from the film through oxidation, as evidenced by the CO_2 partial pressure monitored during the thermal treatment. The ε_∞, which describes the total contribution of the electronic transitions, reduces with temperature but due to different reasons in low- and high-energy IBD films. The $\sigma\rightarrow\sigma^*$ transitions in all films are modified after annealing to 900 °C but strongly at low-energy IBD film where both their transition strength and energy position decreases. In contrary, the $\pi\rightarrow\pi^*$ transitions were less affected in all films. This was attributed (a) to the N redistribution evoluted from sp^3 and sp^2 (in graphitic rings) bonds and bonded mainly in sp^2 bonds, and/or (b) to the formation of sp^2 C═C bonds. Finally, the transition appeared at ~1.6 eV, in high-energy IBD

films reduces considerably after the films' annealing to 900 °C.

In summary, a detailed analysis of the bonding structure of sputtered CN_x films, as affected by the IBD, has been performed by means of the FTIRE technique. The results were discussed through the films electronic behavior as obtained by SE measurements in the NIR-Visible-UV spectral region. The conditions for the formation of hard and elastic three-dimensional carbon-nitrogen bonding structures were clearly correlated to the high-energy IBD. These results can contribute to a further understanding of the bonding mechanisms and electronic modifications during N incorporation in the amorphous carbon matrix and can provide insight towards the production of CN_x films with desired properties, such as fullerenelike films and crystalline C_3N_4 structures.

ACKNOWLEDGMENTS

This work was supported in part by the Greek General Secretariat for Research and Technology under the Project No. PENED-99ED645.

[1] A. Y. Liu and M. L. Cohen, Science **245**, 841 (1989).
[2] A. Y. Liu and M. L. Cohen, Phys. Rev. B **41**, 10 727 (1990).
[3] Y. K. Yap, S. Kida, T. Aoyama, Y. Mori, and T. Sasaki, Diamond Relat. Mater. **8**, 614 (1999).
[4] C. Ronning, H. Feldermann, R. Merk, H. Hofsass, P. Reinke, and J. U. Thiele, Phys. Rev. B **58**, 2207 (1998).
[5] L. R. Shaginyan, A. A. Onoprienko, V. M. Vereschaka, F. Fendrych, and V. G. Vysotsky, Surf. Coat. Technol. **113**, 134 (1999).
[6] T. Szörényi, C. Fuchs, E. Hommet, and F. Le Normand, Surf. Coat. Technol. **125**, 308 (2000).
[7] T. Sebald, R. Kaltofen, and G. Weise, Surf. Coat. Technol. **98**, 1280 (1998).
[8] S. Muhl and J. M. Mendez, Diamond Relat. Mater. **8**, 1809 (1999).
[9] Y. Taki, T. Kitagawa, and O. Takai, Thin Solid Films **304**, 183 (1997).
[10] K. M. Yu, M. L. Cohen, E. E. Haller, W. L. Hansen, and A. Y. Liu, Phys. Rev. B **49**, 2034 (1994).
[11] C. Niu, Y. Z. Lu, and C. M. Lieber, Science **261**, 334 (1993).
[12] D. Marton, K. J. Boyd, A. H. Al-Bayati, S. S. Todorov, and J. W. Rabalais, Phys. Rev. Lett. **73**, 118 (1994).
[13] N. Hellgren, M. P. Johansson, E. Broitman, L. Hultman, and J.-E. Sundgren, Phys. Rev. B **59**, 5162 (1999).
[14] H. Sjöström, S. Stafstrom, M. Boman, J.-E. Sundgren, Phys. Rev. Lett. **75**, 1336 (1995).
[15] H. Sjöström, L. Hultman, J.-E. Sundgren, S. V. Hainsworth, T. F. Page, and G. S. A. M. Theunissen, J. Vac. Sci. Technol. B **14**, 56 (1996).
[16] W. T. Zheng, E. Broitman, N. Hellgren, K. Z. Xing, I. Ivanov, H. Sjöström, L. Hultman, and J.-E. Sundgren, Thin Solid Films **308**, 223 (1997).
[17] R. Kaltofen, T. Sebald, J. Schulte, and G. Weise, Thin Solid Films **347**, 31 (1999).
[18] R. M. A. Azam and H. M. Bashara, *Ellipsometry and Polarized Light* (North Holland, Amsterdam, 1977).
[19] M. Gioti, S. Logothetidis, C. Charitidis, and H. Lefakis, Vacuum **53**, 53 (1999).
[20] J. Fing Phys. Rev. B **30**, 4713 (1984).
[21] P. Kovarik, E. B. D. Bourdon, and R. H. Prince, Phys. Rev. B **48**, 12 123 (1993).
[22] S. Logothetidis, J. Petalas, N. K. Flevaris, and R. L. Johnson, Thin Solid Films **234**, 538 (1993).
[23] S. R. P. Silva, J. Robertson, G. A. J. Amaratunga, B. Rafferty, L. M. Brown, J. Schwan, D. F. Franceschini, and G. Mariotto, J. Appl. Phys. **81**, 2626 (1997).
[24] M. R. Wixom, J. Am. Ceram. Soc. **73**, 1973 (1990).
[25] D. Lin-Vien, N. B. Colthup, W. G. Fateley, and J. G. Grasselli, *The Handbook of Infrared and Raman Characteristic Frequencies of Organic Molecules* (Boston Academic Press, 1991).
[26] Y. Liu, C. Jiaa, and H. Do, Surf. Coat. Technol. **115**, 95 (1999).
[27] J. H. Kaufman, S. Metin, and D. D. Saperstein, Phys. Rev. B **39**, 13 053 (1989).
[28] G. E. Jellison and F. A. Modine, Appl. Phys. Lett. **69**, 371 (1996).
[29] For identification of the $\sigma \rightarrow \sigma^*$ and $\pi \rightarrow \pi^*$ electronic transitions in crystalline graphite, see, for example, Phys. Rev. B **55**, 4999 (1997), and for the $\sigma \rightarrow \sigma^*$ transitions of diamond, **29**, 3470 (1984) and **46**, 4483 (1992).
[30] S. Logothetidis, H. Lefakis, and M. Gioti, Carbon **36**, 757 (1998).
[31] M. Gioti and S. Logothetidis, Diamond Relat. Mater. **8**, 446 (1999).
[32] M. C. dos Santos and F. Alvarez, Phys. Rev. B **58**, 13 918 (1998).
[33] S. Logothetidis, P. Patsalas, and C. Charitidis (unpublished).
[34] R. Prioli, S. I. Zanette, A. O. Caride, M. M. Lacerda, and F. L. Freize Jr., Diamond Relat. Mater. **8**, 993 (1999).
[35] G. L. Chen, Y. Li, J. Lin, C. H. A. Huan, and Y. P. Guo, Diamond Relat. Mater. **8**, 1906 (1999).
[36] In accordance with crystalline graphite where the sp^2 C=C bonds contribute to the $\sigma \rightarrow \sigma^*$ transitions and at an energy of ~2 eV above of the sp^3 carbon-carbon bonds (~12 eV) in diamond, we assume a similar scheme to occur here.